Journal of South American Earth Sciences 121 (2023) 104152

Contents lists available at ScienceDirect

Journal of South American Earth Sciences

journal homepage: www.elsevier.com/locate/jsames

Structure and metamorphism of the Cushamen Complex in Sañicó and Collón Curá-limay rivers confluence: A Devonian metamorphic event related to the subduction stage of the Gondwanan Patagonian orogen

Sebastián Dicaro [a,b,c,*], Santiago N. González [a,c], Samanta Serra-Varela [a,b,c], Nemesio Heredia [d]

[a] Universidad Nacional de Río Negro. Instituto de Investigación en Paleobiología y Geología, Av. Roca 1242, 8332, General Roca, Río Negro, Argentina
[b] Universidad Nacional del Comahue, Facultad de Ingeniería, Depto. de Geología y Petróleo. Buenos Aires 1400, 8300, Neuquén, Argentina
[c] Consejo Nacional de Investigaciones Científicas y Tecnológicas (CONICET). Instituto de Investigación en Paleobiología y Geología. Av. Roca 1242, 8332, General Roca, Río Negro, Argentina
[d] Instituto Geológico y Minero de España, Oviedo Unit, C/Matematico Pedrayes 25, 33005, Oviedo, Spain

ARTICLE INFO

Keywords:
Igneous-metamorphic basement
Paleozoic
North Patagonian Andes
Migmatites
U–Pb zircon geochronology

ABSTRACT

In the North Patagonian Andes and western North Patagonian Massif, the Cushamen Complex is still a matter of interest in order to unravel the Paleozoic evolution of southwestern Gondwana margin. In this contribution we present new petrographic and structural data from the Cushamen Complex cropping out nearby Sañicó town and Collón Curá and Limay rivers confluence together with U–Pb (Q-ICP-MS) detrital zircon ages. In these areas, this metamorphic complex is composed of migmatites, orthogneisses and calcsilicate rocks, with a Late Devonian metamorphic peak age, intruded by Devonian - lower Carboniferous granites. The regional metamorphic peak would also has been accompanied by the development of a pervasive tectonic foliation and associated isoclinal folds. Devonian - Carboniferous granites crosscut the foliation of the migmatites and would have produced a weak contact metamorphism represented by static recrystallization in quartz grains. The regional metamorphic event can be related to the subduction-related Gondwanan orogenic event. At least two more folding phases and related foliations were identified postdating these granitic intrusions, probably related to the collisional event of the Gondwanan orogeny, late Carboniferous - early Permian in age. Evidence of retrograde metamorphism probably related to the previously mentioned foliations and folds are common. Zircons from a mesosome were analyzed by U–Pb Q-ICP-MS yielding a maximum depositional age of 441.79 ± 1.68 Ma (early Silurian/Rhuddanian) indicating a sedimentation for the protholits probably during middle Silurian, age of the pre-orogenic successions of the Gondwanan cycle in Patagonia.

1. Introduction

The Paleozoic basement rocks of the North Patagonian Andes, Precordillera Patagónica, Precordillera Neuquina Sur, Sañicó High and western North Patagonian Massif are constituted by scattered outcrops between 38.8° and 43° S and 68° and 72° W (Fig. 1, Varela et al., 2005, 2015; Pankhurst et al., 2006; Ramos et al., 2011; Serra-Varela et al., 2022 and reference therein). Most of the Paleozoic igneous and metamorphic rocks of the North Patagonian Andes were classically assigned to the Cushamen, Mamil Choique and Lipetrén formations and the Colohuincul Complex (Nullo, 1979; Dalla Salda et al., 1991; Varela et al., 2005, 2015; Cingolani et al., 2011; Marcos et al., 2020 and references therein). The Paleozoic outcrops in the Sañico High are part of the southernmost sector of the Andean Paleozoic basement, located south of 39° S latitude (Heredia et al., 2018). In this sector, three orogenic events have been distinguished: the Famatinian orogeny (Late Ordovician-middle Silurian), the Gondwanan orogeny (Late Carboniferous-early Permian) and the Tabarin orogeny (late Permian-Triassic), according to Heredia et al. (2016, 2018).

Previous works on the deformation, geochronology and metamorphism of the Cushamen Formation (Varela et al., 1991, 2005; Giacosa et al., 2021; Hervé et al., 2005, 2018; Marcos et al., 2020) suggested that this unit was affected by two different metamorphic events developed during the Patagonian Gondwanan orogeny (Serra-Varela et al., 2022). The oldest one is a Devonian - early Carboniferous event linked to an Andean-type subduction orogen (Heredia et al., 2016, 2018;

* Corresponding author. Avenida Roca 1242, 8332, General Roca, Río Negro, Argentina.
E-mail address: sdicaro@unrn.edu.ar (S. Dicaro).

https://doi.org/10.1016/j.jsames.2022.104152
Received 5 September 2022; Received in revised form 2 December 2022; Accepted 6 December 2022
Available online 7 December 2022

Serra-Varela et al., 2022) while the most recent is restricted to the late Carboniferous - early Permian and related to a subsequent collisional orogenic event (Heredia et al., 2016, 2018; Serra-Varela et al., 2022). Nevertheless, most studies have been focused on the latest tectonometamorphic event which is registered in almost all of the basement outcrops related to the Cushamen Formation (see García-Sansegundo et al., 2009 and references therein) and little is known about the oldest one.

The metamorphic rocks outcropping in the Sañicó High near the Collón Curá and Limay rivers confluence and Sañicó town provide an opportunity to study the oldest subduction-related tectonometamorphic event of the Patagonian Gondwanan orogeny. Although geochronological data have already been presented by other authors for this area (Lucassen et al., 2004; Varela et al., 2005; Hervé et al., 2018; Rapela et al., 2022) petrological and structural characterization of these rocks received less attention.

In this paper, new structural, microstructural and petrographic data from the Paleozoic igneous and metamorphic basement rocks, cropping out in the surroundings of Collón Curá and Limay rivers confluence and Sañicó town, are provided. Furthermore, a new U–Pb zircon age for the metamorphic rocks is presented. The integrated data allowed to interpret that the Paleozoic metamorphic rocks in the studied area are affected by at least four composite fabrics, where the second one would have been coeval with anatexis during Late Devonian. This high-grade metamorphism might be related to the early Gondwanan orogeny.

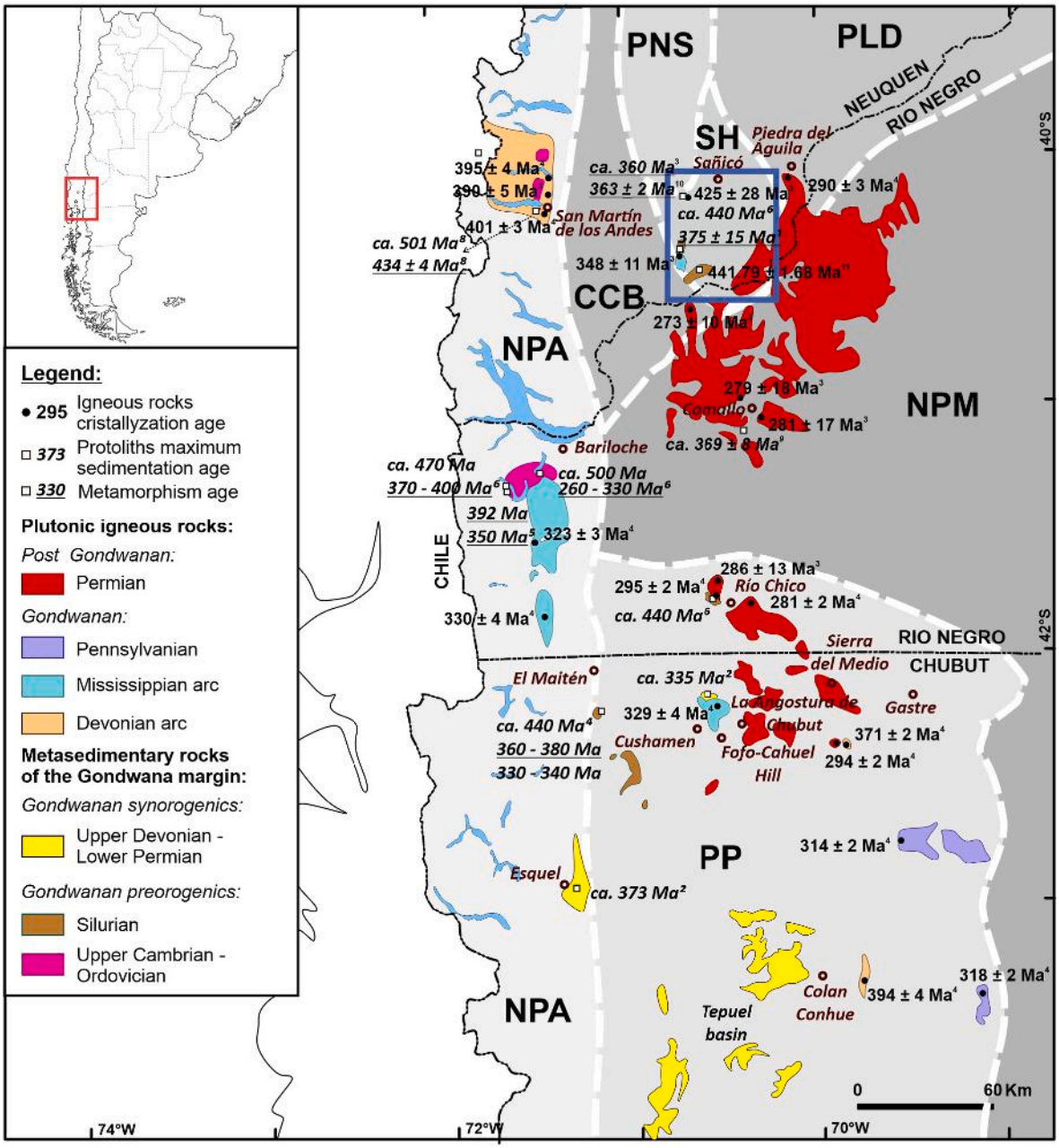

Fig. 1. Simplified geological map showing the distribution of the main Paleozoic igneous and metamorphic basement rocks in northwestern Patagonia. Ages according to: [1]Lucassen et al. (2004); [2]Hervé et al. (2005); [3]Varela et al. (2005); [4]Pankhurst et al. (2006); [5] Martinez et al. (2012); [6]Hervé et al., (2018); [7]Oriolo et al. (2019); [8]Serra-Varela et al. (2019); [9]Marcos et al. (2020); [10]Rapela et al. (2022); [11]this paper. Modified from Serra-Varela et al. (2021). The main morphostructural units, according to Ramos et al. (2011) and Giacosa et al. (2021), are shaded-colored. PNS: Precordillera Neuquina Sur. SH: Sañicó High. PLD: Picún Leufú Depocenter. CCB: Collón Curá Basin. NPA: North Patagonian Andes. NPM: North Patagonian Massif. PP: Precordillera Patagónica. Location of Fig. 2 is shown in blue square.

Moreover, the new U–Pb zircon age enabled to propose a maximum depositional age of 441.79 ± 1.68 Ma for the protolith of these metamorphic rocks.

2. Geological setting

The Cushamen Formation was originally defined by Volkheimer (1964) as phyllites and metaquartzites with minor amount of migmatites, cropping out to the southeast of El Maitén, near the confluence of the Ñorquincó and Cushamen streams. Nevertheless, gneisses, schists, migmatites, meta-igneous and calcsilicate rocks outcropping along the areas of Cushamen, Río Chico, La Angostura de Chubut, Huancache range, Fofo-Cahuel hill, Sierra del Medio, Sañicó, Collón Curá and Limay rivers confluence, Piedra del Águila, Paso Flores and Comallo were also included in this lithostratigraphic unit (Varela et al., 1991, 2005; Dalla Salda et al., 1994; Cerredo, 1997; Giacosa et al., 2021; Marcos et al., 2020; González and Giacosa, 2021) (Fig. 1).

Recently, Serra-Varela et al. (2022) renamed the Cushamen Formation as Cushamen Complex due to its varied lithological composition, as well as its deformational style and metamorphic characteristics. Furthermore, two tectonometamorphic events were distinguished for the Cushamen Complex linked to different geotectonic settings. The first one would correspond to a Middle - Late Devonian to early Carboniferous subduction related event (Heredia et al., 2016, 2018) and the second one, developed between late Carboniferous and the early Permian (García-Sansegundo et al., 2009; Lopez de Luchi et al., 2010; Lucassen et al., 2004; Pankhurst et al., 2006; Varela et al., 1991, 2005), and related to a collisional event (Heredia et al., 2016, 2018). Moreover, the sedimentation age of the protoliths of this complex has been proposed from middle Silurian (Wenlock) to lower Carboniferous (Hervé et al., 2005,2018; Pankhurst et al., 2006; Marcos et al., 2020; Serra-Varela et al., 2022). This complex was affected by a wide range of P-T conditions, varying from greenschist to upper amphibolite facies (Cerredo, 1997; Dalla Salda et al., 1994) that would have triggered anatexis proved by the presence of migmatites in the Collón Curá and Limay rivers confluence and Comallo areas (Varela et al., 1991, 2005; Marcos et al., 2020). In this work, we will refer to this unit as the Cushamen Complex, as proposed by Serra-Varela et al. (2022).

The Cushamen Complex is intruded by igneous rocks related to four late Paleozoic magmatic events (Pankhurst et al., 2006). The three oldest events are related to the Gondwanan cycle (Heredia et al., 2016, 2018; Serra-Varela et al., 2019, 2022) and their rocks can be included in the Mamil Choique Formation. The oldest late Paleozoic magmatic event has been dated between 401 and 371 Ma (Devonian I-Type granitoids) and represents the main Gondwanan magmatic event (Pankhurst et al., 2006; Heredia et al., 2016, 2018; Serra-Varela et al., 2019). The intermediate event has been dated between 350 and 323 Ma (early Carboniferous I-type granitoids) and between *ca.* 320–290 Ma (late Carboniferous-early Permian S-Type granitoids; Pankhurst et al., 2006). The last magmatic Paleozoic event is younger than *ca.* 290 Ma (Permian-Triassic S- to I-Type granitoids), representing the post-Gondwanan magmatism. The Gondwanan I-Type granitoids form two separate alignments with NNW-SSE trends where the Devonian alignment seems to be located to the east of the early Carboniferous alignment (Serra-Varela et al., 2019, 2021). According to Heredia et al. (2016, 2018) and Serra-Varela et al. (2019, 2021, 2022), the I-Type granitoids (Devonian to early Carboniferous) are related to the development of the Gondwanan subduction magmatic arc and the S-Type granitoids with the Gondwanan collisional event.

The structural features of the Cushamen Complex have been described by several authors (Giacosa et al., 2021; von Gosen, 2009; Serra-Varela et al., 2018; Marcos et al., 2020). Regionally, these rocks show a complex fabric, being a pervasive tectonic foliation the conspicuous one (S_2), although a relictic foliation (S_1) has been also described. The pervasive foliation contains the metamorphic peak mineral assemblage, and it is related to tight and isoclinal folds (axial plane foliation). In some localities this planar fabric is affected by open folds producing crenulation which results in a new foliation. Despite the similarities among the different outcropping sites, the S_1 and S_2 foliations and associated folds, are mostly linked to a Carboniferous - Permian event (López de Luchi et al., 2006; García-Sansegundo et al., 2008; Marcos et al., 2020; Serra-Varela et al., 2022).

In the Bariloche area, metamorphic rocks included in the Colohuincul Complex (Cambrian - Ordovician), show similar structures as the late Carboniferous - early Permian ones affecting the Cushamen Complex (Serra-Varela et al., 2022). In addition, the metamorphic peak, related to the ductile fabrics that affect these outcrops is constrained between the Late Pennsylvanian and the Cisuralian (García-Sansegundo et al., 2009; Oriolo et al., 2019), age of the collisional event of the Patagonian Gondwanan orogeny. This would indicate the absence of the Famatinian Patagonian orogeny (Upper Ordovician-middle Silurian) in these rocks and their location in the western foreland of the Famatinian orogen (Serra-Varela et al., 2019, 2022).

3. Local geology

The studied area is located southeastward of the Precordillera Neuquina Sur, at the Sañicó High (Ramos et al., 2011) (Fig. 1). The Paleozoic basement of the area consists of igneous and metamorphic rocks (Fig. 2) covered by Triassic - Early Jurassic epiclastic and volcaniclastic deposits of the Paso Flores and Sañico formations and crosscut by Miocene basalts assigned to the Cerro Petiso Formation (Cucchi et al., 1998; Escosteguy et al., 2013).

The basement rocks in this region comprise gneisses, schists, migmatites and calcsilicate rocks intruded by Paleozoic granites (Lucassen et al., 2004; Varela et al., 1991, 2005; Rapela et al., 2022). The metamorphic rocks of the Sañicó area are mostly composed of tonalitic orthogneisses and scarce meta-diorites that yielded a crystallization age of 425 ± 28 Ma (U–Pb on zircons; Varela et al., 2005). For the Collón Curá and Limay rivers confluence area, the age of the metamorphic peak was calculated in 375 ± 15 Ma (U–Pb on titanite, Lucassen et al., 2004). Moreover, for the Sañicó area, close to Collón Curá area, the metamorphic peak age yielded values between 363 ± 2 Ma (U–Pb SHRIMP on zircon, Rapela et al., 2022) and *ca.* 360 Ma (U–Pb on titanite, Varela et al., 2005). These metamorphic peak ages (Late Devonian) of the Gondwanan metamorphism coincide with the Gondwanan Patagonian magmatic arc, mainly developed in Devonian - early Carboniferous times (Heredia et al., 2016, 2018; Serra-Varela et al., 2021). The Paleozoic granites that intrude the metamorphic rocks, close to the confluence of the Collón Curá and Limay rivers were defined as anatectic and syntectonic granitoids (Varela et al., 1991). One of these plutonic rocks yielded an age of 348 ± 11 Ma (U–Pb in zircons, Varela et al., 2005), in agreement with the age of the second Gondwanan magmatic event of Pankhurst et al. (2006) related to the final stages of the Gondwanan subduction (Serra Varela et al., 2019, 2021).

The gneisses and schists were originally included in the Cushamen Formation by Varela et al. (1991, 2005), while the migmatites and granites were assigned to the Mamil Choique and Lipetrén formations (Ravazzoli and Sesana, 1977; Nullo, 1979; Escosteguy et al., 2013, among others), Devonian - lower Permian and Permian - Triassic, respectively. Nevertheless, in the redefinition of the Cushamen Formation as a metamorphic complex, Serra-Varela et al. (2022) included the migmatites in the Cushamen Complex.

4. Results

4.1. Migmatites

These rocks consist in stromatitic metatexites and schollen and schlieric diatexites (Fig. 3) where stromatitic metatexites are the most abundant lithology. They are represented by schistose and gneissic mesosomes intercalated with granitic leucosomes and biotitic

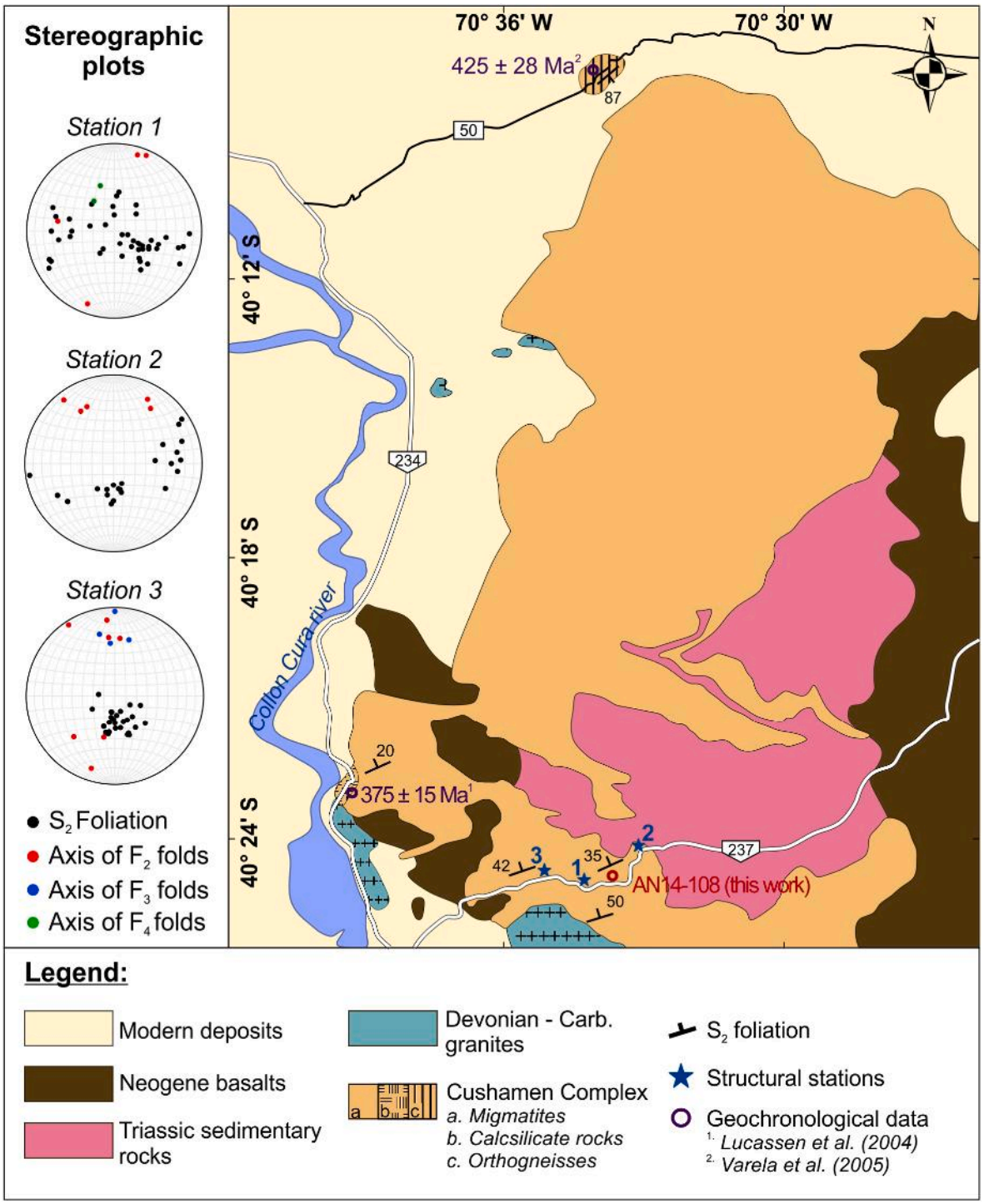

Fig. 2. Geological map of the studied area showing the main lithostratigraphic units as well as stereographic plots for the main structures. Modified from Escosteguy et al. (2013). Lower hemisphere equal area projection of poles to S_2 are represented in the stereographic plots.

melanosomes (Fig. 3a and b). The intercalation of leucosomes, mesosomes and melanosomes, as well as a spaced to continuous schistosity of the mesosomes and other features described in section 4.4, give rise to a pervasive axial plane tectonic foliation (S_2) (Fig. 3a and b). The diatexites (Fig. 3c and d) are less common compared to the metatexites. Their mineral association consists of Qtz + Kfs + Pl + Bt (Abbreviations according to Siivola and Schmidt, 2007). Modal variation of alkaline feldspar and plagioclase leads to compositions ranging from granitic to granodioritic. Schlieren found in these rocks are composed of Bt + Grt. Quartz-rich rafts were also identified with lenticular to angular morphologies. The diverse content of schlieren and rafts led to the development of schollen and schlieric diatexites within single outcrops (Fig. 3d). Locally, some schollen diatexites showed metatexite rafts (Fig. 3c). Biotite aggregates and garnet with biotite reaction rims were found in both types of diatexites.

In the metatexites, the mesosomes are usually tabular granolepidoblastic schists and gneisses (Fig. 3a, b, 4a and 4b) with minor exceptions of angular shapes with extents close to 1 m. On the other hand, scarce oblate and prolate quartz-rich mesosome bodies were identified in the metatexitic migmatites. Two characteristic mineral associations were

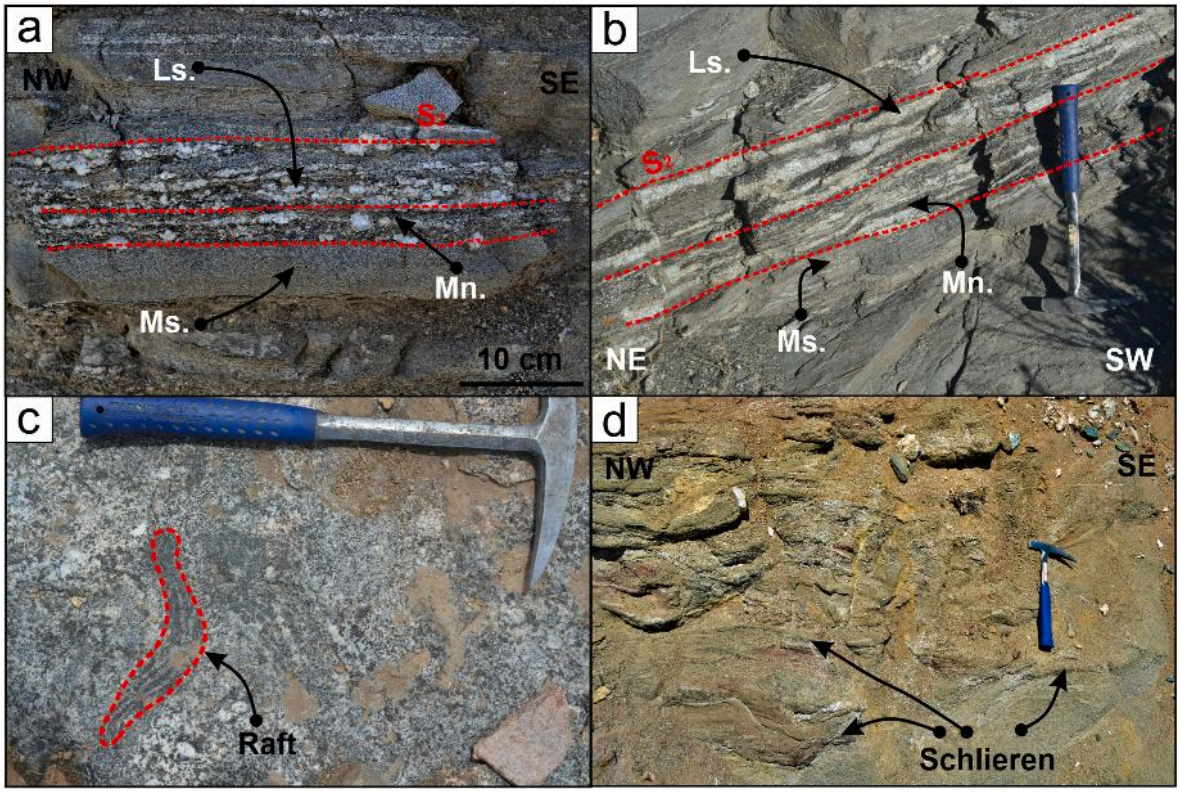

Fig. 3. Field photographs of the migmatite outcrops. a and b: Metatexites. The red dashed lines mark the pervasive foliation S_2 given by the mesosomes (Ms), leucosomes (Ls) and melanosomes (Mn). c: Schollen diatexites showing a metatexite raft. d: Schlieric diatexites.

identified in gneisses and schists: Qtz + Pl + Bt ± Grt ± Kfs (Fig. 4b and c) and Qtz + Bt + Sil ± Grt ± Pl (Fig. 4d to f). The sillimanite is commonly present as fibrous to prismatic inclusions in muscovite patches (Fig. 4d and e). Garnet was found sporadically as inclusions in plagioclases.

The leucosomes are white to pink and exhibit coarse-grained equigranular to pegmatitic textures (Fig. 5). The morphology of the leucosomes varies from lenticular to tabular with an average thickness of 5 cm (Fig. 3a and b). Some of them are collected by subvertical to subhorizontal bodies with an average thickness of 20 cm (Fig. 5a). However, few subhorizontal leucosomes with thickness reaching 1.5 m were identified (Fig. 5b). The leucosomes are harmonic with respect to S_2 foliation. The subhorizontal bodies are parallel to S_2, while the subvertical ones are mostly oblique to S_2. The lenticular leucosomes also converge in similar structures with length/width ratios close to 1 (Fig. 5c). Moreover, two structures related to the anatexis were found such as ptygmatic folds and collapse structures by melt loss (Bons et al., 2008) (Fig. 5d and e). The former structures include leucosomes and melanosomes. The melanosomes consist of biotite aggregates and subordinated garnets. The development of these thin mafic layers is not only restricted to the leucosome limits, as they constitute schlieren within the leucosomes (Fig. 5f). The mineralogy of the leucosomes consists of Qtz + Pl + Bt + Ms ± Kfs ± Grt (Fig. 6a and b). Euhedral garnets that reach sizes up to 1.5 cm are present in a significant number of leucosomes (Fig. 6c). Several of these crystals developed reaction rims mostly of biotite (Fig. 6b and c) and to a lesser extent plagioclase (Fig. 6d). Mirmekytes in feldspars as well as quartz symplectites in muscovite were found (Fig. 6e and f). Flame perthites are present in alkaline feldspar (Fig. 6g). Biotite is partially replaced by chlorite and surrounded by muscovite rims (Fig. 6h).

4.2. Orthogneisses and calcsilicate rocks

Tonalitic orthogneisses, cropping out discontinuously nearby Sañicó, are composed of plagioclase, quartz and biotite. These rocks contain mafic microgranular enclaves with rounded to angular shapes with sizes up to 30 cm (Fig. 7a and b). They are locally crosscut by tonalitic to granitic veins.

The calcsilicate rocks consist in lentiform structures of different length (mostly centimetric to decimetric) aligned following the pervasive foliation (S_2) of the schist that hosts them (Fig. 7c). The calcsilicate lenses present black reaction rims of hornblende as a classical metamorphic reaction with the siliciclastic (Al-rich) host rock (Fig. 7c and d). The calcsilicate rocks are composed of Qtz + Pl + Zo + Tr-Act + Hbl + Ttn ± Cal (Fig. 7e and f). This lithology is also present within the metatexites and could be considered as a resister.

4.3. Igneous rocks

The igneous rocks are mainly constituted by granites that intrude the migmatites and even include them as pendants (Fig. 8a). They are composed of quartz, plagioclase, alkaline feldspars, muscovite and biotite (Fig. 8b). These intrusive rocks cut the main tectonic foliation (S_2) of the metamorphic rocks (Fig. 8c to e), defining sharp contacts and develop two different shapes: (1) small magma batches (Fig. 8c) with extensions ranging from few meters to several tens of meters and (2) tabular bodies with thicknesses up to 20 cm (Fig. 8d). Undeformed pegmatitic granitic dyke swarms (Fig. 8e) crosscut the migmatites, calcsilicate rocks and granites.

The small magma batches developed textural zoning and modal and grain size bandings (Fig. 8b and c). Textural zoning consists of medium to coarse grain cores which shift abruptly to pegmatitic borders. The bandings consist of alternating fine-grained with coarse-grained bands (Fig. 8b). The fine-grained bands have elevated modal contents of biotite

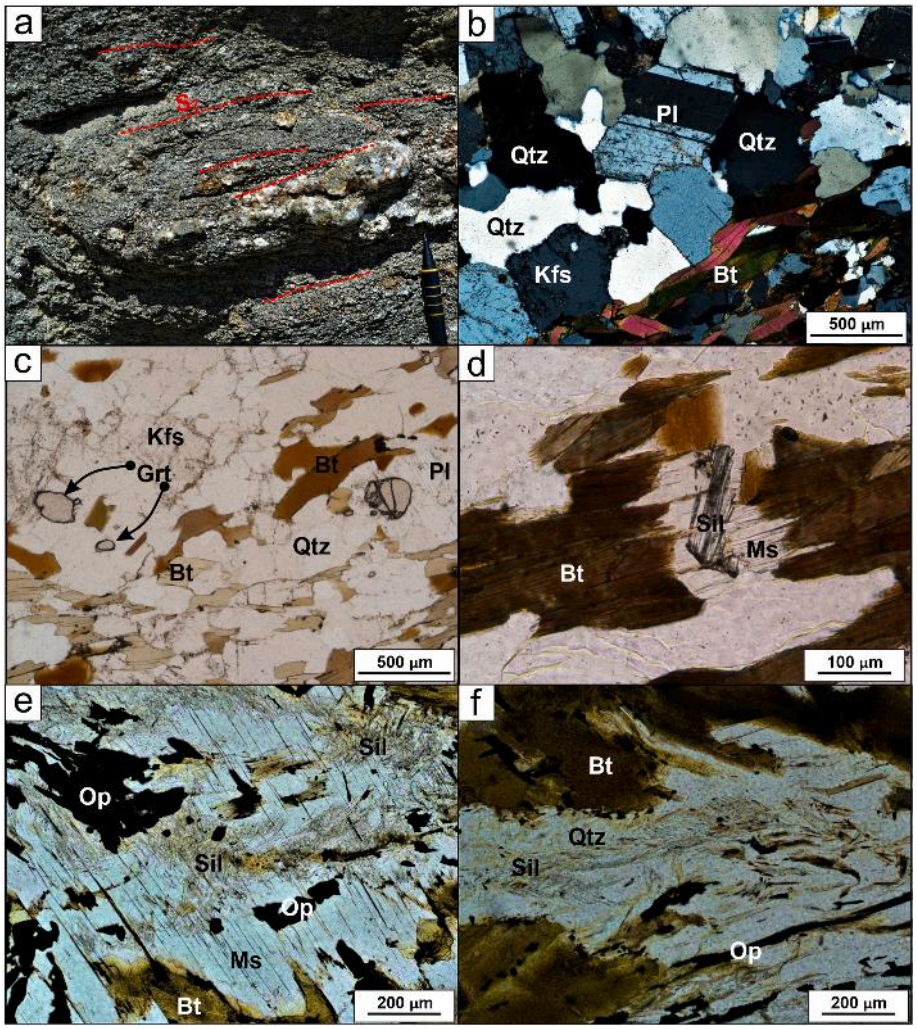

Fig. 4. Field photographs and photomicrographs of mesosomes in metatexites. a: Bt-rich Schistose mesosomes. Red dashed lines mark the pervasive foliation S_2 given by platy minerals. b: Cross-polarized light photomicrograph of gneissic mesosome composed by Pl + Kfs + Qtz + Bt. c: Plane-polarized light photomicrograph of gneissic mesosome composed by Pl + Bt + Qtz + Kfs + Grt. d: Plane-polarized light photomicrograph of gneissic mesosome with sillimanite. e: Plane-polarized light photomicrograph of schistose mesosome with sillimanite in muscovite patches. f: Plane-polarized light photomicrograph of schistose mesosome with sillimanite in quartz.

which are arranged parallel to the banding. In these igneous bodies, enclaves of the metatexitic host rocks can be found with their internal foliation parallel to the granite/host rock contact. Locally, quartz is present as polygonal grains and develops undulose extinction. These granites show a disjunctive tectonic foliation, given by fractures, parallel to the enclave's foliation (Fig. 8a). Centimetric pegmatitic dykes crosscut both structures.

The mineralogical composition of the intrusive tabular bodies (2) is similar to that of the small magma batches, except for their higher proportion of perthitic K-feldspar. These rocks crosscut the migmatites. They are medium to coarse grained and locally pegmatitic (Fig. 8d). The tabular bodies show textural and compositional bandings, with quartz, K-feldspar and plagioclase coarse grained bands intercalated with fine grain bands with the same mineralogy but including biotite (Fig. 8d).

4.4. Structure

At least four tectonic foliations can be recognized in the studied area. The main structure developed in the metamorphic rocks can be identified as a pervasive axial plane tectonic foliation (S_2) (Figs. 4a, 8c and 8e and 9a). S_2 develops as compositional and grain size bandings, preferred orientation of platy (Bt, Ms and Sil) and lenticular mineral aggregates or a combination of these features. It is also common to identify S_2 in the metatexites as a banding given by the leucosomes, mesosomes and melanosomes (Fig. 3a, b and 9a). This foliation strikes ENE-WSW and dips mainly between 15° and 50° north-northwest and subordinately 50°–70° to the northeast (Fig. 2). Nevertheless, it displays a wide variation in orientation between outcrops probably due to posterior deformation. A relictic tectonic foliation (S_1), was identified only in thin sections as polygonal arcs in biotite (Fig. 9b) contained in the pervasive foliation (S_2), constituting, in most cases, a composite foliation (S_2+S_1).

The metatexites are folded at different scales. Open to tight folds at outcrop scale were identified, concentrating the leucosomes in the fold hinges. The axial planes of isoclinal centimetric folds (F_2) in the leucosomes and mesosomes are parallel to the S_2 foliation (Fig. 9a). The axes of the isoclinal folds dip between 35° and 50° mainly to the NNW, although SSE and SSW plunges were also measured (Fig. 2). These folds are refolded into tight angular folds (F_3) (Fig. 9c and d). F_3 develop an associated crenulation cleavage (S_3) in the schistose paleosomes (Fig. 9d, e and 9f). S_2 is locally transposed by the latter producing narrow zones of a composite foliation (S_3+S_2+S_1) (Fig. 9e and f). These structures are refolded by open folds (F_4) with NW-NNW dipping axes that define a rough axial plane cleavage (S_4), oblique to orthogonal to S_3, given by incipient chlorite growth (Fig. 9e to g). The latter folds develop mushroom shapes patterns that resemble Ramsay type 2 interference patterns (Fig. 9e and f).

Most leucosomes present boudinage structures, developing beaded morphologies. The melanosomes developed a foliation (S_2) that consists in preferred orientated biotites. Some of these minerals are strongly flexured with centimetric folds (F_3) whose hinges present fractured garnets. Locally, minor centimetric shear zones were found in fold limbs, evidenced by the presence of sigma structures in plagioclases (Passchier

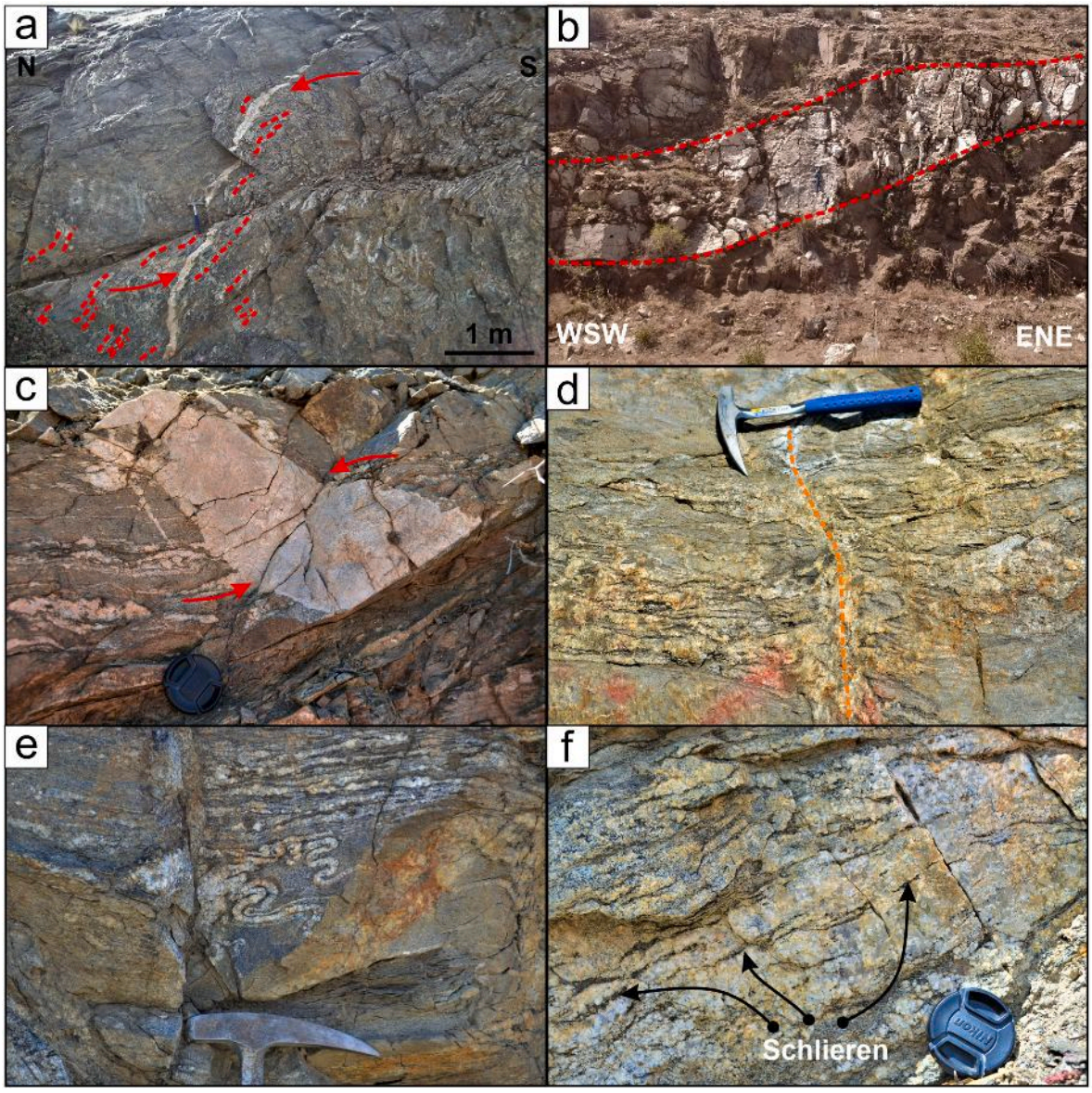

Fig. 5. Field photographs showing different structures in leucosomes. a: Subvertical leucosome. Red arrows show smaller leucosomes (red dashed lines) converging in it. b: Tabular leucosome with thicknesses up to 150 cm. Red dashed lines mark the limits of the tabular body. c: Lenticular leucosome corresponding to a dilatant zone. Red arrows show smaller leucosomes converging in it. d: Collapse structure by melt loss marked by orange dashed line. e: Ptygmatic folds. f: Biotite schlierens in leucosome.

and Trouw, 2005). These structures are parallel to the S_2 foliation.

While the S_2 foliation affects the metamorphic rocks, the early Carboniferous igneous rocks are not affected by this foliation. Nevertheless, these igneous rocks are affected by a posterior tectonic fabric (Fig. 8a) which could be related to either the S_3 or S_4 foliations.

Numerous faults crosscut both igneous and metamorphic rocks and their respective fabrics at high angles (>50°). These brittle structures dip mostly to the west, although north and northwest dips were also identified. Drag folds are associated with high angle faults (Fig. 9h). On the other hand, centimetric faults crosscut some leucosomes.

4.4.1. Microstructures

Multiple microstructures that evidence dynamic recrystallization in quartz and feldspar were identified in the leucosomes of the metatexites. Quartz presents grain boundary migration, subgrain rotation and chessboard extinction (Fig. 10a and b) (Passchier and Trouw, 2005). Limited polygonal quartz grains were also found. Plagioclase exhibits bulging, quartz simplectites and polysynthetic curved and tapered twins (Fig. 10c). Kinking was identified in scarce biotite (Fig. 10d) and muscovite crystals. The microstructures in quartz and plagioclase suggest that the metatexites would have been affected by high temperature dynamic recrystallization processes. Subgrain rotation and grain boundary migration in quartz would indicate temperatures ranging between 400° and 500 °C for the former microstructure and temperatures from 500° to 700 °C for the latter (Passchier and Trouw, 2005). Bulging in plagioclase would represent dynamic recrystallization in a temperature range of 450°–600 °C (Passchier and Trouw, 2005). On the other hand, polygonal quartz grains would evidence local static recrystallization.

The gneissic mesosomes show the same microstructures in quartz and plagioclase described for the leucosomes (Fig. 10e and f, respectively). At microscale, the principal foliation in these rocks is expressed by a compositional banding of quartzfeldspatic bands and biotite-rich bands. Some single crystals of this phyllosilicate are found scattered and parallel-oriented in the quartzfeldspatic bands (Fig. 10g). Locally, the gneissic mesosome foliation is represented by the orientation of

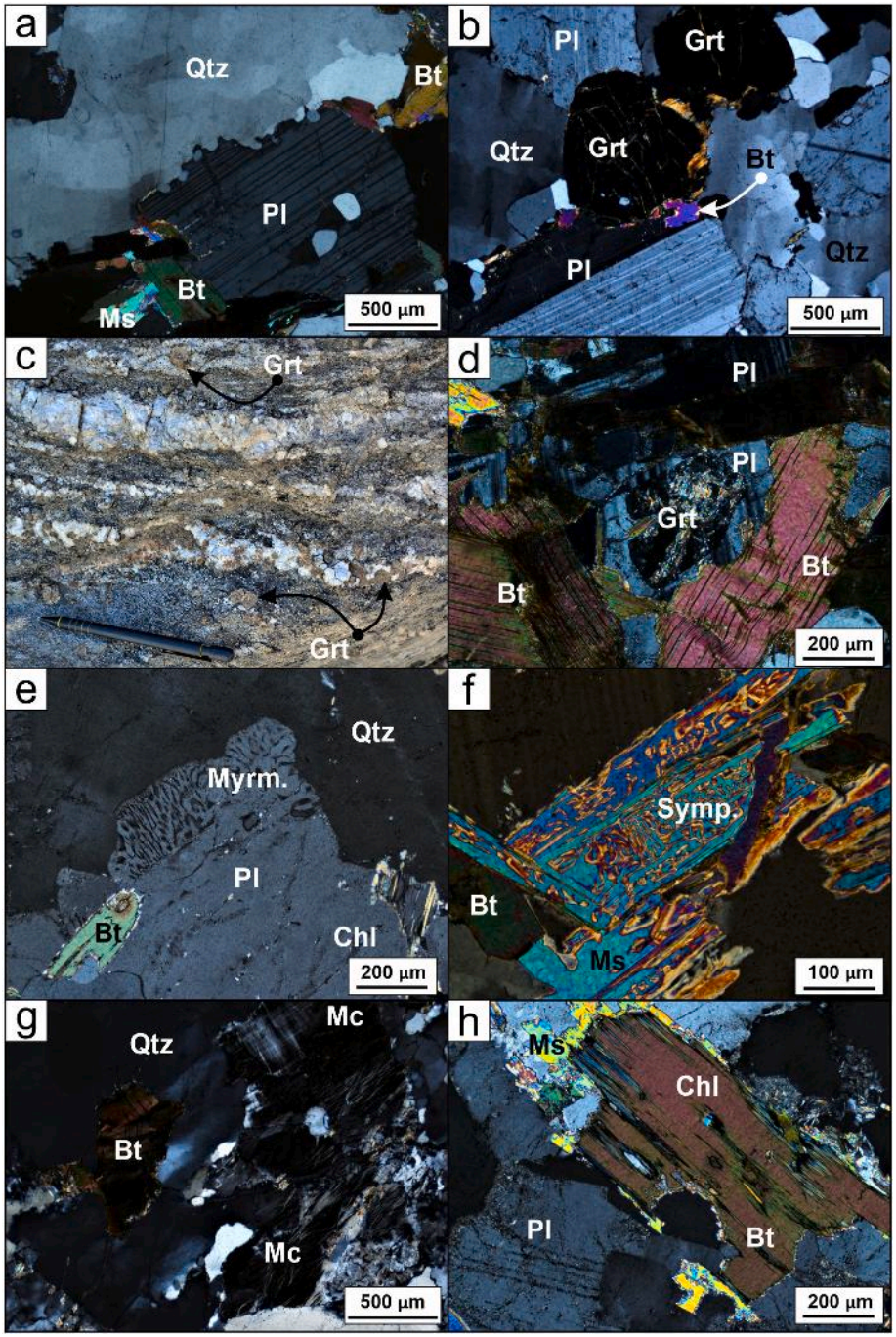

Fig. 6. Photomicrographs of leucosomes and melanosomes mineralogy and textures. a: Cross-polarized light photomicrograph of Qtz + Pl + Bt + Ms leucosome. b: Cross-polarized light photomicrograph of Qtz + Pl + Bt + Grt leucosomes. Note the incipient rims of biotite around the garnets. These biotites are partially replaced by chlorite. c: Field photograph of garnets in leucosomes. Note the biotite rim around the garnet pointed by the black arrow at the top of the photograph. d: Cross-polarized light photomicrograph of plagioclase rims around garnets in melanosomes. e: Cross-polarized light photomicrograph of myrmekitic texture (Myrm.). f: Cross-polarized light photomicrograph of quartz symplectites (symp.) in muscovite. g: Cross-polarized light photomicrograph of flame perthites in alkaline feldspars and kinking in biotite. h: Cross-polarized light photomicrograph of muscovite rims around biotite. The latter is also partially replaced by chlorite.

quartz and/or feldspar microlithons (Fig. 10h). Polygonal arc microstructures were identified in biotite aggregates.

The schistose mesosomes present a foliation that consists in preferred orientation of Ms + Qtz + Grt + Sil aggregates with lenticular shapes. These aggregates are included in a matrix composed of muscovite, quartz and other phyllosilicates. The matrix and the inner zones of the aggregates developed a crenulation cleavage represented by the axial plane of angular microfolds. Garnet contained in the aggregates are intensely fractured, while the sillimanite is flexured. As well as in the gneissic mesosomes, biotite in the schistose mesosomes form polygonal arc microstructures. The crenulation cleavage orientation correlates with the orientation of the principal pervasive axial plane foliation described for the metatexites (S_2). Numerous muscovite patches were identified in these schists.

5. U–Pb zircon analysis

5.1. Methodology

Sample AN14-108 (Figs. 1 and 2; 40° 24.963′ S – 70° 33.662’ W) is a mesosome from a metatexite where no leucosome was collected in the sample. It is a granolepidoblastic schist with a paragenesis of Bt + Pl + Qtz and accessory opaque minerals and zircon. This sample was collected to assess the maximum depositional age as well as the detrital pattern of the sample.

Standard jawcrushing, sieving and heavy mineral concentration by hydraulic processes were performed at the laboratories of the Instituto de Paleobiología y Geología (Universidad Nacional de Río Negro). Zircon grains were handpicked under a binocular microscope. One

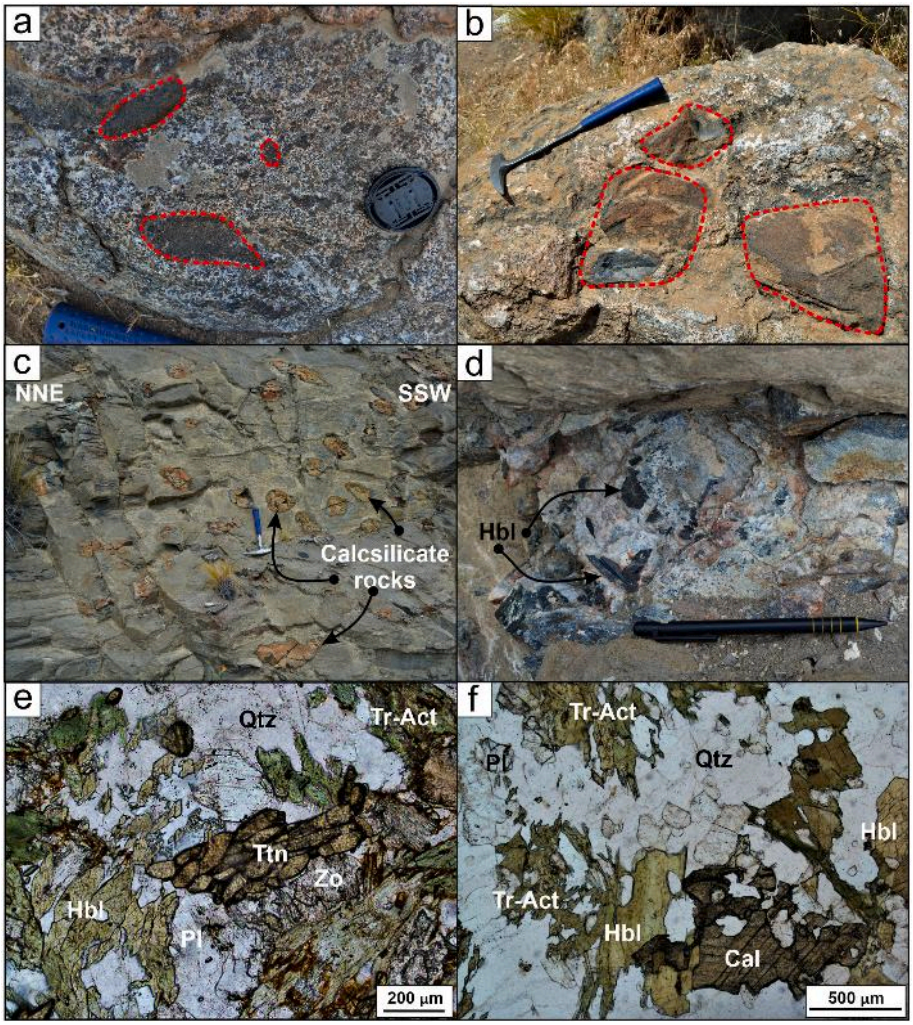

Fig. 7. Field photographs and photomicrographs of orthogneisses and calcsilicate rocks. a and b: Mafic microgranular enclaves in orthogneisses. c: Lenticular calcsilicate rocks hosted by schists. d: Large hornblende crystals within calcsilicate rocks. e: Plane-polarized light photomicrograph of Qtz + Pl + Hbl + Tr-Act + Zo + Ttn mineral assemblage of the calcsilicate rocks. f: Plane-polarized light photomicrograph of Pl + Tr-Act + Hbl + Cal + Qtz mineral assemblage of the calcsilicate rocks included as resisters within the metatexites.

hundred and fifty of these grains were mounted in epoxy resin and polished. Backscattered electron images (BSE) were obtained with a JEOL JSM 5600 scanning electron microscope of the Universidad de Oviedo, in order to assess the internal morphology, prior to the U–Pb laser work. U–Pb analyses were performed in SGIker Institute (Universidad del País Vasco) using a quadrupole mass spectrometer with inductively coupled plasma source (Q-ICP-MS) Thermo Fisher Scientific, XSeries-II model coupled to a New Wave UP213 laser ablation system. Laser spot size was 30 μm. Data were acquired during a 30 s background measurement followed by 60 s ablation of the sample. Laser-induced elemental fractionation and instrumental mass discrimination were corrected by normalization to the reference zircon GJ-1 (Jackson et al., 2004) as primary standard, and Plesovice reference zircon as secondary standard (Sláma et al., 2008). The measure sequence among standard samples is a standard followed by 5 unknowns. For data treatment, we used the Iolite 3 software (Paton et al., 2011) and VizualAge (Petrus and Kamber, 2012). Age calculation and plots were made using IsoplotR software (Vermeesch, 2018). For further details of the analytic procedures see Puelles et al. (2014). All analytical errors are presented as absolute values at 2σ level (Results in supplementary data, Table 1).

5.2. Detrital zircon analysis

Seventy-six zircons were analyzed from this sample out of which eight were discarded for being discordant and having high common Pb contents. Based on the shape of the crystals, different zircon groups were identified: euhedral zircons with lengths between 90 and 160 μm and ratios of 2:1 to 3:1; subhedral zircons with lengths between 80 and 130 μm and rounded zircons with lengths up to 130 μm and aspect ratios of 1:1 (Fig. 1 in supplementary data).

Out of the sixty-eight concordant zircons the main provenance is Upper Ordovician - Lower Silurian, being the main peak in the distribution at 441 Ma (Fig. 11). The youngest zircon ages (396 Ma and 411 Ma) might be interpreted as a partial resetting product of metamorphism since their Th/U ratio is below 0.1 (Lucassen et al., 2004; Rapela et al., 2022). Other important groups of ages are early Cambrian - Ediacaran, Neoproterozoic and Mesoproterozoic with peaks in the distribution at 610 Ma and 1100 Ma. Also, there are single analyses of 1852, 2637 and 2736 Ma (Fig. 11).

A maximum deposition age was estimated considering the weighted mean age of the 10 youngest concordant zircons. Discarding the two youngest single zircons as metamorphic, the weighted mean age is 441.79 ± 1.68 Ma (Fig. 11c) while the youngest zircon in the cluster is 421 ± 18 Ma. We interpreted this weighted mean age as the most plausible maximum depositional age for the protoliths of the Cushamen Complex in the study area.

6. Discussion

6.1. Deformation and metamorphism

There is a complex relationship between the tectonometamorphic events and the lithologies in the Cushamen Complex of the studied area. The relictic foliation S_1 is only present as polygonal arcs in biotite within

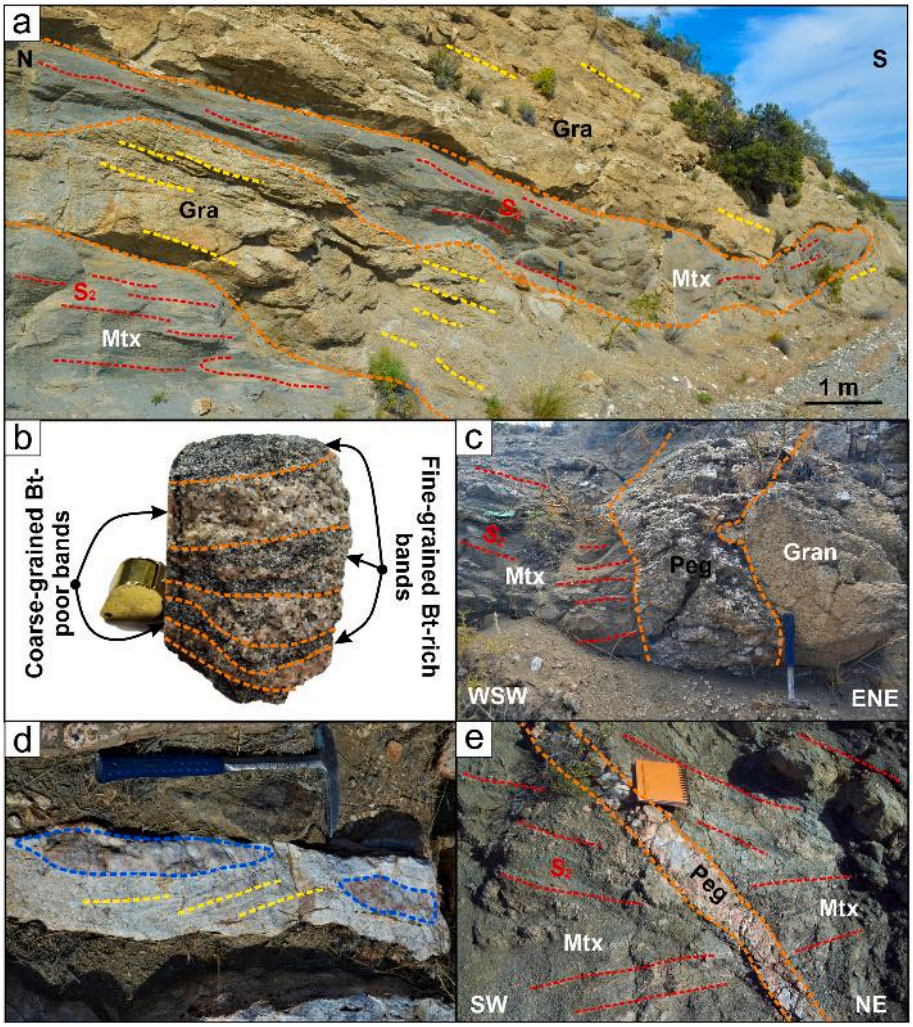

Fig. 8. Field photographs of geological relationships between granites and metamorphic rocks. a: Tabular metatexite enclaves (Mtx) in the Devonian granite (Gra). Yellow dashed lines show the disjunctive tectonic foliation of the granite. Orange dashed lines mark the limit between granites and migmatites. Red dashed lines show the pervasive foliation S_2 of the migmatites. b: Grain-size and mineral banding (orange dashed lines) in the granites. c: Zoned Devonian granite intruded in the metatexites. Coarse-grained core (Gran) and pegmatitic borders (Peg). Orange dashed lines mark the limit between granites and migmatites. Red dashed lines show the pervasive foliation S_2 of the migmatites. d: Tabular granites with grain-size banding (yellow dashed lines) and local sites with pegmatitic textures (light-blue dashed lines). e: Pegmatitic dyke crosscutting the metatexites ductile fabric. Orange dashed lines mark the limit between granites and migmatites. Red dashed lines show the pervasive foliation S_2 of the migmatites.

the S_2 foliation at microscopic scale and no signs of a low grade paragenesis could be found which could be interpreted as an obliteration of the low grade paragenesis by a high grade one. The S_2 foliation is an axial plane foliation defined by parallel growth of Bt + Ms ± Sil ± Grt which is the high-grade paragenesis found in the mesosomes of the migmatitic rocks (Figs. 4 and 9b). Moreover, leucosomes in metatexites are mostly parallel to this foliation. Intrafolial and isoclinal folds F_2 are found in association to the composite S_2+S_1 foliation. This foliation might be the product of transposition during coaxial progressive deformation (Fig. 9a). This fabric might be linked to the high temperature dynamic recrystallization microstructures such as grain boundary migration in quartz and bulging in plagioclase (Passchier and Trouw, 2005). On the other hand, lenticular leucosomes with length/width ratios close to 1 and minor leucosomes converging in them, could be interpreted as dilatant sites or dilatant zones (Sawyer, 2008). The S_1 and S_2–F_2 structures might be restricted to the Late Devonian – early Carboniferous Gondwanan subduction-related orogeny (Heredia et al., 2016, 2018), as these structures do not affect the granites.

Late tight folds F_3 refold the previous structures (Fig. 9c and d). The crenulation of S_2, as seen in biotite-rich melanosomes and mesosomes, can be linked to F_3. This crenulation affects the metamorphic peak paragenesis and, hence, would have postdated the migmatization. F_4 was described for the migmatites as open folds (Fig. 9g) that affect the previous structures and develop Ramsay type 2 interference patterns (Fig. 9e and f). The F_3 and F_4 postdate the metamorphic peak. Nevertheless, it is not clear if both structures succeed the early Carboniferous granitic intrusions, since the disjunctive cleavage observed in the granites could be related to either of them, as the granites only crosscut the S_2.

The presence of sillimanite indicates that the metamorphic peak reached by these rocks corresponds to the sillimanite isograd (upper amphibolite facies). Additionally, the identified dynamic recrystallization microstructures in the migmatites and the development of partial melting processes supports this metamorphic grade. On the other hand, the polygonal quartz grains generated in the metamorphic rocks can be attributed to a static recrystallization process that could have been originated by the thermal effect related to the intrusion of the early Carboniferous granites. The latter structures were also recognized in the granites and might be related to a grain boundary area reduction process (Passchier and Trouw, 2005).

The mineral association found in the calcsilicate rocks of Pl + Qtz + Zo + Tr-Act + Ttn + Cal ± Hbl indicates that these rocks would have reached the zoisite zone (Winter, 2014), represented by the reaction: An + Cal + H_2O = Zo + CO_2. This metamorphic zone could be compared to the garnet zone and the previously mentioned amphibolite facies in terms of temperature and pressure.

Several pieces of evidence support that a retrograde metamorphism affected the migmatites. The scarce sillimanite in the leucosomes is partially to totally replaced by muscovite patches (Fig. 4e and f). Flame perthites occur in feldspars in rocks deformed under greenschist facies (Fig. 6g) (Passchier and Trouw, 2005). Biotite replaced by chlorite and muscovite rims also implies retrograde metamorphism under low grade

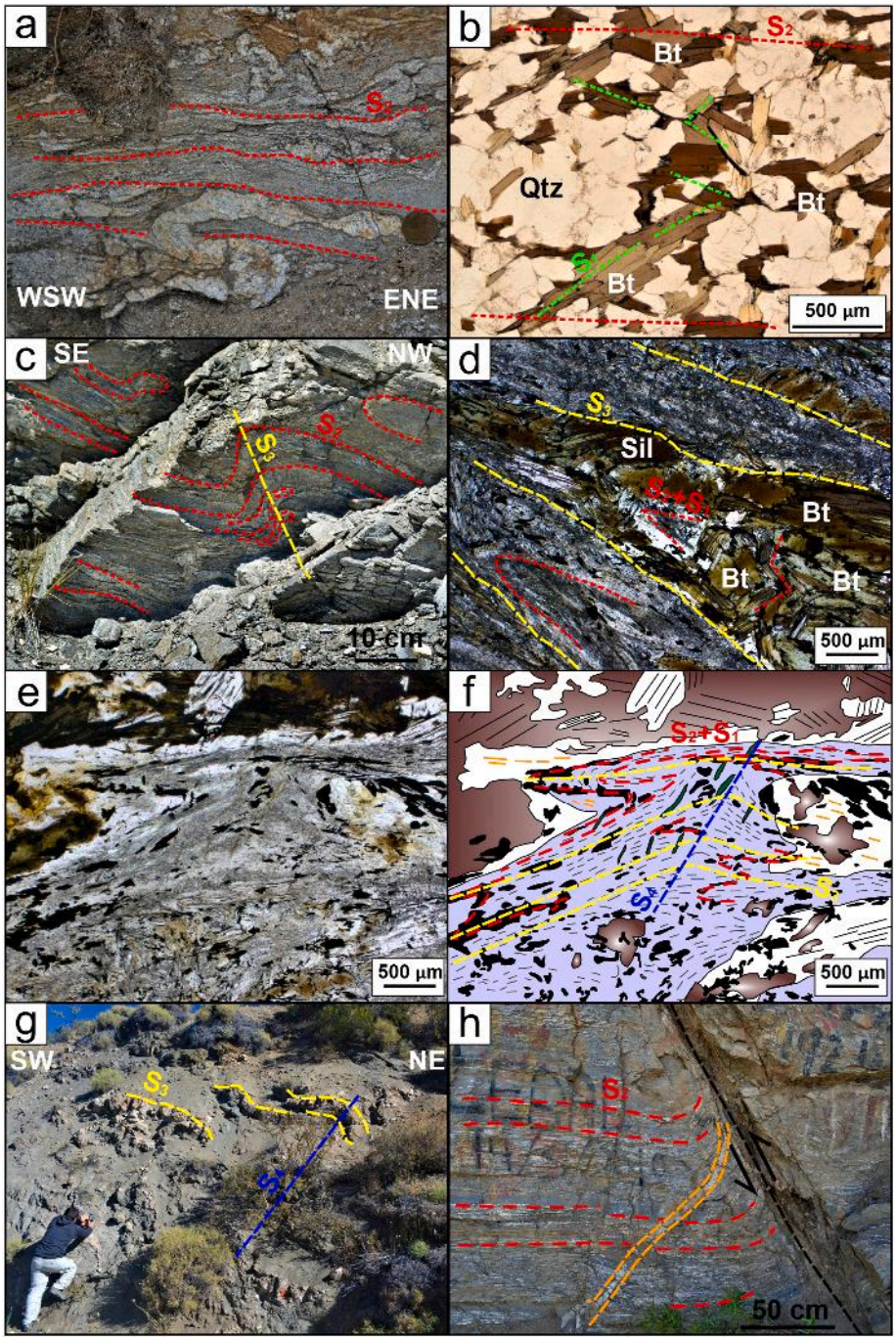

Fig. 9. Structural features. a: Field photograph of pervasive S_2 foliation (red dashed lines) and isoclinal intrafolial F_2 folds. b: Plane-polarized light photomicrograph of relictic foliation S_1 (green dashed lines) as polygonal arcs in biotite. Red dashed line shows S_2. c: Field photograph of S_2–F_2 (red dashed lines) refolded structures into F_3 folds. Yellow dashed lines show the foliation S_3. d: Plane-polarized light photomicrograph of schistose mesosome. Yellow dashed lines mark S_3 foliation. S_2+S_1 (red dashed lines) is preserved as polygonal arcs in biotite. Sillimanite aggregates are flexured following S_2+S_1. e: Plane-polarized light photomicrograph of schistose mesosome showing a complex structural pattern. f: schematic interpretation of (e). Brown diffused polygons represent biotite aggregates. White polygons represent muscovite patches. Gray polygons represent the matrix. Black polygons represent opaque minerals. Green polygons represent chlorite aggregates. Orange lines represent sillimanite aggregates. Gray lines represent fine-grained phyllosilicates within the matrix. Red dashed lines represent foliation S_2+S_1. Yellow dashed lines represent S_3+S_2+S_1 foliation. Blue dashed line represents the foliation S_4. g: Field photograph of composite foliation S_3 (yellow dashed lines) folded into F_4 folds. Blue dashed line represents foliation S_4. h: Reverse fault (black dashed line) and related drag folds affecting the migmatites (red dashed lines represents the pervasive foliation S_2) and granites (orange dashed lines).

conditions (Fig. 6h). Moreover, rehydration reactions were also recorded in muscovite by the presence of quartz simplectites in these phyllosilicates (White et al., 2005) (Fig. 6f). Plagioclase rims were present around a few garnet crystals, which suggests a rapid decompression (Stowell and Stein, 2005) for the migmatites (Fig. 6d).

6.2. Geological evolution

A geological evolution for the metamorphic Cushamen Complex of this area can be proposed taking into account all the data collected. Based on the petrographic and structural features of these metamorphic rocks together with the wide spectra of detrital ages obtained from the geochronological analysis (see supplementary data, Table and Fig. 1) the protolith can be inferred as a sedimentary sequence that includes pelites, graywackes and marls intruded by tonalitic igneous rocks. The banding given by the leucosomes and melanosomes with the mesosomes can be attributed to differences in the susceptibility to partial melting of the protolith. Such differences can be explained by a protolith constituted by a sequence of pelites and greywackes, where the pelites would be more susceptible to anatexis. The crosscutting relationships between the orthogneisses and the migmatites remain unclear, as the outcrops of the former are discontinuous and scarce. Notwithstanding, Rapela et al. (2022) interpreted a metamorphic age of 363 ± 2 Ma for an orthogneiss of the Cushamen Complex, based on Th/U ratios from zircons, inferring that the emplacement of this intrusion might have been synchronous with the metamorphism.

Considering the maximum depositional age calculated for the metasedimentary sequence, sedimentation of the Cushamen Complex in the

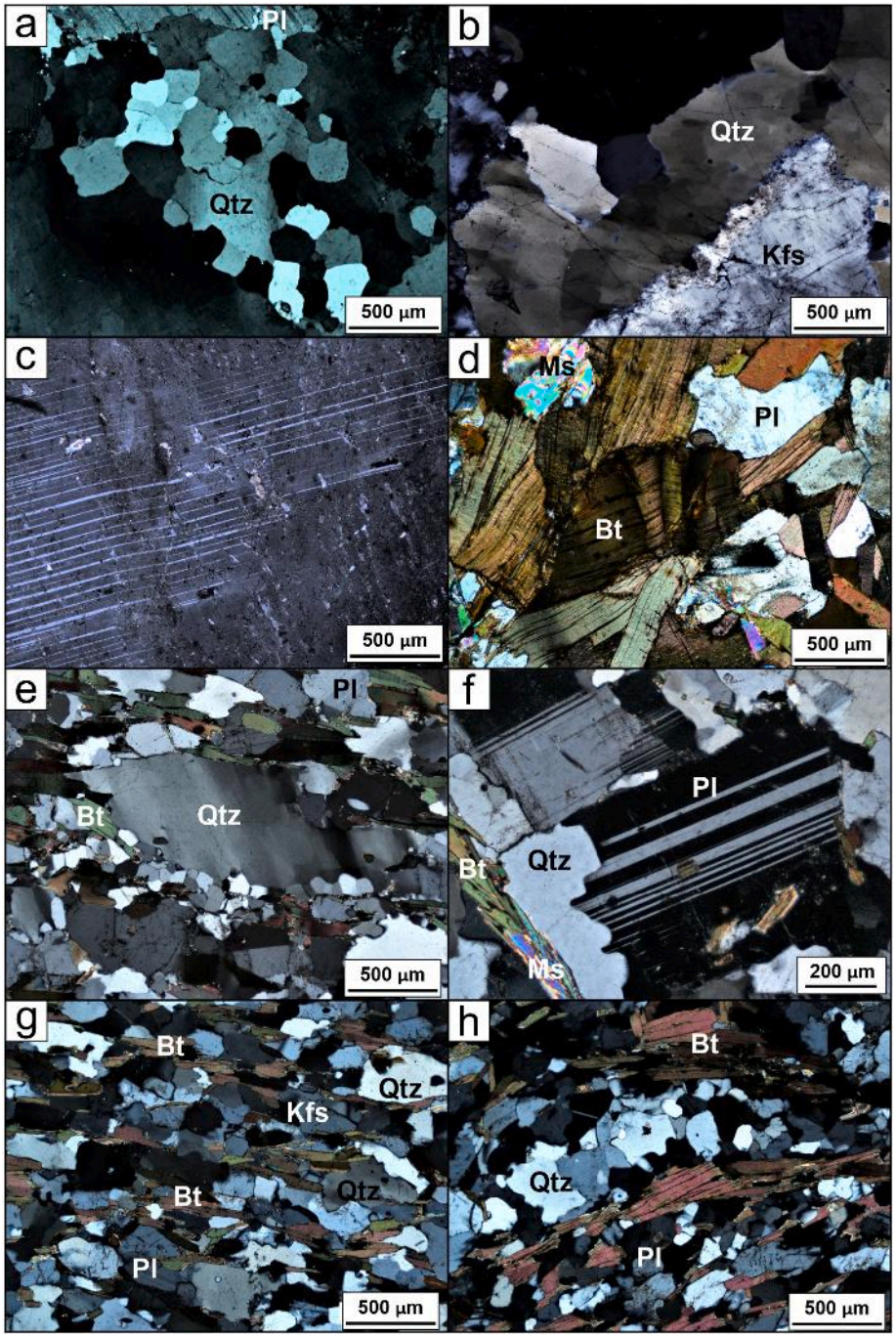

Fig. 10. Metatexites microestructures. a: Grain boundary migration in quartz within the leucosomes. b: Chessboard extinction in quartz from the leucosomes. c: Curved and tapered twins in plagioclase from the leucosomes. d: Kinking in biotites from the melanosomes. E to h represent microstructures from the mesosomes. e: Subgrain rotation in quartz. f: Bulging in plagioclase. g: Scattered biotite crystals parallel-oriented in the quartzfeldspatic bands. h: Quartz microlithons surrounded by biotites representing the cleavage domains. Quartz develops grain boundary migration.

studied area should have happened at approximately 441.79 ± 1.68 Ma or younger, probably during middle Silurian. This age is coherent with the detrital age calculated by Hervé et al. (2018) for this basement where they found the youngest provenance peak at *ca.* 440 Ma. Nevertheless, they propose a post-Ordovician, possibly Devonian sedimentation age. Moreover, Serra-Varela et al. (2022) proposed a middle Silurian (Wenlock) to early Carboniferous age for the Cushamen Complex, based in the ages of the post-Famatinian deposits in Patagonia.

On the other hand, the granites in this area yielded ages of 348 ± 11 (U–Pb in zircons, Varela et al., 2005). These granites crosscut the S_2 foliation of the metamorphic basement rocks with sharp defined contacts. This age sets up a limit for the metamorphic event as older than early Carboniferous. Also, Hervé et al. (2018) found detrital zircons with ages between *ca.* 365 to 320 Ma with high common Pb which they interpreted as being rejuvenated ages due to the effect of intrusive igneous rocks. U–Pb ages in titanite from the calcsilicate rocks and a metadiorite were calculated in 375 ± 15 and *ca.* 360 Ma, respectively, and interpreted as the peak of the metamorphic event (Lucassen et al., 2004; Varela et al., 2005). The composite foliation S_2 and the coeval folds (F_2) would have developed under these metamorphic conditions.

The undeformed pegmatitic granite dykes that crosscut the migmatites and granites are still a matter of interest, as they are post-Carboniferous, but no geochronological data is available. Based only on field relationships, they can be related to the last magmatic Paleozoic event, Permian in age (post-orogenic Gondwanan event) (Pankhurst et al., 2006).

The retrograde metamorphism under greenschist conditions, interpreted from the exposed pieces of evidence, could have been related to

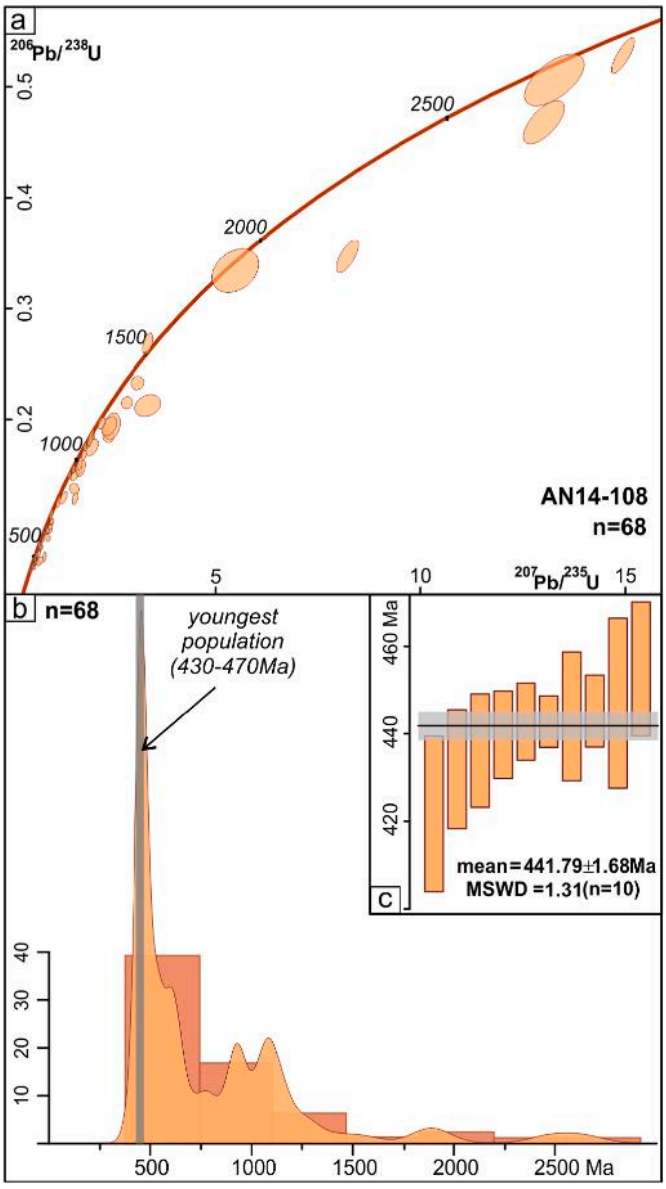

Fig. 11. Concordia diagram (a) and frequency histogram (b) for analyzed zircons from sample AN14-108. c: Weighted mean age for the ten youngest concordant zircons.

S_3–F_3 and/or S_4–F_4 fabric since the former contains muscovite patches and the latter contains incipient chlorite. Finally, the west dipping faults and associated drag folds, that crosscut S_2–F_2 and S_3–F_3 structures and the granites, would have taken place under brittle conditions postdating the high-grade metamorphism and carboniferous magmatism. In addition, the latter structures might be linked to the Andean cycle.

7. Conclusions

This integrated petrographic, structural, microstructural and geochronological study has made a contribution towards a better understanding of the tectonometamorphic evolution of the Cushamen Complex. This led to the following concluding remarks:

(1) The protoliths of the Cushamen Complex in the studied area would have consisted in a sedimentary sequence of graywackes, pelites and minor marls intruded by tonalitic igneous bodies. Based on detrital zircons, the sedimentation would have taken place at approximately 441.79 ± 1.68 Ma or younger, probably in Middle Silurian (Wenlock) times.

(2) The Cushamen Complex in the studied area was affected by an upper amphibolite grade metamorphism that triggered anatectic processes related to a metamorphic peak with a Late Devonian age (*ca.* 380–360). This anatexis would have happened contemporaneously with a pervasive S_2–F_2 ductile tectonic fabric. The S_1 (relict) and S_2 fabrics do not affect the lower Carboniferous igneous rocks (348 ± 11 Ma) and can be linked to the Late Devonian – early Carboniferous Gondwanan subduction-related orogeny, in close association with the Gondwanan magmatic arc.

(3) The S_3–F_3 and S_4–F_4 would postdate the metamorphic peak and affect the metamorphic and igneous rocks. Consequently, these structures would be at least early Carboniferous and probably related to the end of the subduction-related Gondwanan orogeny or, either, with its final collisional event, late Carboniferous-early Permian in age.

(4) The basement rocks cropping out nearby Collón Curá and Limay rivers confluence and Sañicó town described in this paper constitute the perfect place to study and unravel the tectonometamorphic evolution of the Cushamen Complex during the oldest stage of the subduction-related Gondwanan Patagonian orogeny.

CRediT authorship contribution statement

Sebastián Dicaro: Writing – review & editing, Writing – original draft, Visualization, Methodology, Investigation. **Santiago N. González:** Writing – review & editing, Writing – original draft, Supervision, Resources, Methodology. **Samanta Serra-Varela:** Writing – review & editing, Writing – original draft, Visualization, Supervision, Resources. **Nemesio Heredia:** Writing – review & editing, Supervision, Resources, Funding acquisition.

Declaration of competing interest

The authors declare that they have no known competing financial interests or personal relationships that could have appeared to influence the work reported in this paper.

Data availability

No data was used for the research described in the article.

Acknowledgements

This work has been supported by the projects TORANDES (CGL 2012-38396-C03) of the Spanish I + D + i Plan with FEDER Funds of the European Union. The authors thank for technical and human support provided by SGIker of UPV/EHU and European funding (ERDF and ESF).

The authors would like to thank Andrés Folguera (editor), as well as Sebastián Cao and Carlos Fernández (reviewers) whose comments and suggestions have greatly enhanced this manuscript.

Appendix A. Supplementary data

Supplementary data to this article can be found online at https://doi.org/10.1016/j.jsames.2022.104152.

References

Bons, P.D., Druguet, E., Castaño, L., Elburg, M.A., 2008. Finding what is now not there anymore: recognizing missing fluid and magma volumes. Geology 36, 851–854.

Cerredo, M.E., 1997. The metamorphism of Cushamen Formation, Río Chico área. North patagonian Massif, Argentina. 8° Congreso Geológico Chileno, Actas (2), 1236–1240.

Cingolani, C.A., Zanettini, J.C., Leanza, H.A., 2011. El Basamento Ígneo Metamórfico. En. In: Leanza, H., Arregui, C., Carbone, O., Danieli, J.C., y Vallés, J. (Eds.). Geología

y Recursos Naturales de la Provincia del Neuquén. 18° Congreso Geológico Argentino, Relatorio, pp. 37–47.
Cucchi, R., Espejo, R., González, R., 1998. Hoja Geológica 4169-I, Piedra del Águila. Programa Nacional de Cartas Geológicas de la República Argentina 1:250.000. Provincias de Río Negro y Neuquén. Instituto de Geología y Recursos Minerales. Servicio Geológico Minero Argentino. Boletin 242, 1–74 (Buenos Aires).
Dalla Salda, L.H., Cingolani, C., Varela, R., 1991. El basamento pre-andino ígneo metamórfico de San Martín de los Andes, Neuquén. Rev. Asoc. Geol. Argent. 46, 223–234.
Dalla Salda, L.H., Varela, R., Cingolani, C., Aragón, E., 1994. The rio Chico paleozoic crystalline complex and the evolution of northern Patagonia. J. S. Am. Earth Sci. 7, 377–386.
Escosteguy, L., Geuna, S., Franchi, M., González Díaz, E., Dal Molin, C., 2013. Hoja Geológica 4172-II San Martín de los Andes. Provincias de Neuquén y Río Negro. In: Servicio Geológico Minero Argentino. Boletín, vol. 409. Instituto de Geología y Recursos Minerales, Buenos Aires, pp. 1–92.
García-Sansegundo, J., Cuesta, A., Farias, P., Gallastegui, G., Heredia, N., Giacosa, R., 2008. La estructura de la región de Río Chico (Macizo Norpatagónico, Argentina). 17° Congreso Geológico Argentino, Actas, pp. 67–68.
García-Sansegundo, J., Farias, P., Gallastegui, G., Giacosa, R.E., Heredia, N., 2009. Structure and metamorphism of the gondwanan basement in the Bariloche region (North Patagonian Argentine Andes). Int. J. Earth Sci. 98 (7), 1599–1608.
Giacosa, R.E., González, S.N., Greco, G.A., 2021. Regiones Geológicas. In: Giacosa, R.E. (Ed.). Geología yRecursos Naturales de la Provincia de Chubut. Relatorio del 21° Congreso Geológico Argentino, Relatorio, pp. 34–44.
González, P.D., Giacosa, R.E., 2021. Rocas metamórficas e ígneas del Paleozoico. In: Giacosa, R.E. (Ed.). Geología y Recursos Naturales de la Provincia de Chubut. Relatorio 21° Congreso Geológico Argentino, Relatorio, pp. 47–104.
Heredia, N., Garc, a-Sansegundo, J., Gallastegui, G., Farias, P., Giacosa, R., Alonso, J.L., Busquets, P., Charrier, R., Clariana, P., Colombo, F., Cuesta, A., Gallastegui, J., Giambiagi, L., González-Menéndez, L., Limarino, C.O., Martín-González, F., Méndez-Bedia, I., Pedreira, D., Quintana, L., Rodríguez-Fernández, L.R., Rubio-Ordoñez, A., Seggiaro, R., Serra-Varela, S., Spalletti, L., Cardó, R., Ramos, V.A., 2016. Evolución Geodinámica de los Andes argentino-chilenos y la Península Antártica durante el Neoproterozoico tardío y el Paleozoico. Trabajos de Geología, Universidad de Oviedo 36, 237–278.
Heredia, N., García-Sansegundo, J., Gallastegui, G., Farias, P., Giacosa, R., Hongn, F., Tubía, J.M., Juis Alonso, J., Busquets, P., Charrier, R., Clariana, P., Colombo, F., Cuesta, A., Gallastegui, J., Giambiagi, L., González-Menéndez, L., Limarino, O., Martín-González, F., Pedreira, D., Quintana, L., Rodríguez-Fernández, L.R., Rubio-Ordoñez, A., Seggiario, R., Serra-Varela, S., Spalletti, L., Cardó, R., Ramos, V.A., 2018. The pre-andean phases of construction of the southern Andes basement in neoproterozoic-paleozoic times. In: Folguera, A., Contreras Reyes, A., Heredia, N., Encinas, A., Oliveros, V., Dávila, F., Collo, G., Giambiagi, L., Maksymowicz, A., Iglesia Llanos, M.P., Turienzo, M., Naipauer, M., Orts, D., Litvak, V., Alvarez, O., Arriagada, C. (Eds.), The Evolution of the Chilean-Argentinean Andes. Springer-Verlag, Switzerland, pp. 111–131.
Hervé, F., Haller, J.M., Duhart, P., Fanning, C.M., 2005. SHRIMP U-Pb Ages of Detrital Zircons from Cushamen and Esquel Formations, North Patagonian Massif, Argentina: Geological Implications. 16° Congreso Geológico Argentino, Actas, pp. 309–314.
Hervé, F., Calderón, M., Fanning, C.M., Pankhurst, R.J., Rapela, C.W., Quezada, P., 2018. The country rocks of devonian magmatism in the North Patagonian Massif and chaitenia. Andean Geol. 45, 301–317.
Jackson, S.E., Pearson, N.J., Griffin, W.L., Belousova, E.A., 2004. The application of laser ablation-inductively coupled plasma-mass spectrometry to in situ U-Pb zircon geochronology. Chem. Geol. 211 (1–2), 47–69.
López de Luchi, M.L., Cerredo, M.E., Wemmer, K., 2006. Time constraints for the tectonic evolution of the SW corner of the North Patagonian Massif, Argentina. Fifth South American Symposium on Isotope Geology, Punta del Este, Uruguay Short Papers 221.
Lopez de Luchi, M.G., Cerredo, M.E., Martínez Dopico, C., 2010. Lithology and age of the Cushamen Formation. Devonian magmatism in the western North Patagonian Massif. Argentina. Bolletino di Geofisica teorica ed applicata 51, 71–74.
Lucassen, F., Trumbull, R., Franz, G., Creixell, C., Vásquez, P., Romer, R.L., Figueroa, O., 2004. Distinguishing crustal recycling and juvenile additions at active continental margins: the Paleozoic to recent compositional evolution of the Chilean Pacific margin (36-41°S). J. S. Am. Earth Sci. 17, 103–119.
Marcos, P., Pivetta, C.P., Benedini, L., Gregori, D.A., Geraldes, M.C., Scivetti, N., Barros, M., Varela, M.E., Dos Santos, A., 2020. Late Paleozoic geodynamic evolution of the western North Patagonian Massif and its tectonic context along the southwestern Gondwana margin. Lithos 1–19, 376-377.
Martínez, J.C., Dristas, J.A., Massone, H.J., 2012. Palaeozoic accretion of the microcontinen Chilenia, North Patagonian Andes: high-pressure metamorphism and subsequent thermal relaxation. Int. Geol. Rev. 54 (4), 472–490.
Nullo, F.E., 1979. Descripción geológica de la hoja 39c, Paso Flores. Carta Geológico-Económica de la República Argentina. Escala 1:200.000. Provincia de Río Negro, vol. 167. Servicio Geológico Nacional, Boletín, Buenos Aires, pp. 1–78.
Oriolo, S., Schulz, B., González, P.D., Bechis, F., Olaizola, E., Krause, J., Renda, E., Vizán, H., 2019. The late paleozoic tectonometamorphic evolution of Patagonia revisited: insights from the pressure-temperature-deformation-time (P-T-D-t) path of the gondwanide basement of the North Patagonian cordillera (Argentina). Tectonics 38, 2378–2400.
Pankhurst, R.J., Rapela, C.W., Fanning, C.M., Márquez, M., 2006. Gondwanide continental collision and the origin of Patagonia. Earth Sci. Rev. 76, 235–257.
Passchier, C.W., Trouw, R.A.J., 2005. 2nd Revised and Enlarged Edition. Springer/Verlag Berlin, pp. 1–366.
Paton, C., Hellstrom, J., Paul, B., Woodhead, J., Hergt, J., 2011. Iolite: freeware for the visualization and processing of mass spectrometric data. J. Anal. At. Spectrom. 26, 2508–2518.
Petrus, J.A., Kamber, B.S., 2012. VizualAge: a novel approach to laser ablation ICP-ms U-Pb geochronology data reduction. Geostand. Geoanal. Res. 36 (3), 247–270.
Puelles, P., Abalos, B., García de Madinabeitia, S., Sánchez-Lorda, M.E., Fernández-Armas, S., Gil Ibarguchi, J.I., 2014. Provenance of quartz-rich metamorphic tectonite pebbles from the Black Flysch (W Pyrenees, N Spain): an EBSD and detrital zircon LA-ICP-MS study. Tectonophysics 632 (C), 123–137.
Ramos, V.A., Folguera, A., García Morabito, E., 2011. Las provincias geológicas del Neuquén. In: Leanza, H., Arregui, C., Carbone, O., Danieli, J.C., y Vallés, J. (Eds.). Geología y Recursos Naturales de la Provincia del Neuquén. Relatorio 18° Congreso Geológico Argentino, Relatorio, pp. 317–326.
Rapela, C.W., Hervé, F., Pankhurst, R.J., Calderón, M., Fanning, C.M., Quezada, P., 2022. The Chaitenia Accretionary Orogen of Northwest Patagonia: New U-Pb SHRIMP Ages of the Foreland Basin. Actas del 21° Congreso Geológico Argentino, pp. 1511–1512.
Ravazzoli, I.A., Sesana, F.L., 1977. Descripción geológica de la hoja 41c, Rio Chico. Carta Geológico-Económica de la República Argentina. Escala 1:200.000. Provincia de Rio Negro, vol. 148. Servicio Geológico Nacional. Boletín, Buenos Aires, pp. 1–82.
Sawyer, E., 2008. Atlas of Migmatites. The Canadian Mineralogist, Special Publication 9. NRC Research Press, Ottawa, Ontario, Canada, pp. 1–371.
Serra-Varela, S., González, S.N., Dicaro, S., Heredia, N., Giacosa, R., 2018. El basamento polideformado en la confluencia de los Ríos Limay y Collón Curá, borde noroccidental del Macizo Nordpatagónico, provincia de Neuquén. In: XVII Reunión de Tectónica: La Rioja, Comisión de Tectónica de la Asociación Geológica Argentina.
Serra-Varela, S., González, S.N., Giacosa, R.E., Heredia, N., Pedreira, D., Martín-González, F., Sato, A.M., 2019. Evolution of the Palaezoic basement of the Northpatagonian Andes in the San Martín de los Andes area (Neuquén, Argentina): petrology, age and correlations. Andean Geol. 46, 102–130.
Serra-Varela, S., Heredia, N., Giacosa, R., García-Sansegundo, J., Farias, P., 2022. Review of the polyorogenic Palaeozoic basement of the Argentinean North Patagonian Andes: age, correlations, tectonostratigraphic interpretation and geodynamic evolution. Int. Geol. Rev. 64 (1), 72–95.
Serra-Varela, S., Heredia, N., Otamendi, J., Giacosa, R., 2021. Petrology and geochronology of the San Martín de los Andes batholith: insights into the Devonian magmatism of the North Patagonian Andes. J. S. Am. Earth Sci. 109, 1–20.
Siivola, J., Schmid, R., 2007. List of mineral abbreviations. Classification and glossary of terms. Recommendations of the International Union of Geological Sciences 93–110.
Sláma, J., Kosler, J., Condon, D.J., Crowley, J.L., Gerdes, A., Hanchar, J.M., Hanchar, J. M., Horstwood, M., Morris, G., Nasdala, L., Norberg, N., Schaltegger, U., Schoene, B., Tubrett, M., Whitehouse, M.J., 2008. Plesovice zircon-A new natural reference material for U-Pb and Hf isotopic microanalysis. Chem. Geol. 249 (1–2), 1–35.
Stowell, H., Stein, E., 2005. The significance of plagioclase-dominant coronas on garnet, Wenatchee Block, Northern Cascades, Washington, U.S.A. Can. Mineral. 43, 367–385.
Varela, R., Dalla Salda, L., Cingolani, C., Gomez, V., 1991. Estructura, petrología y geocronología del basamento de la región del Limay, Provincias de Rio Negro y Neuquén, Argentina. Rev. Geol. Chile 18 (2), 147–163.
Varela, R., Basei, M.A.S., Cingolani, C.A., Siga Jr., O., Passarelli, C.R., 2005. El basamento cristalino de los Andes Norpatagónicos en Argentina: geocronología e interpretación tectónica. Rev. Geol. Chile 32 (2), 167–187.
Varela, R., Gregori, D.A., González, P.D., Basei, M.A.S., 2015. Caracterización geoquímica del magmatismo de arco devónico y carbonífero-pérmico en el noroeste de Patagonia, Argentina. Rev. Asoc. Geol. Argent. 72 (3), 419–432.
Vermeesch, P., 2018. IsoplotR: a free and open toolbox for geochronology. Geosci. Front. 9, 1479–1493. https://doi.org/10.1016/j.gsf.2018.04.001.
Volkheimer, W., 1964. Estratigrafía de la zona extrandina del Departamento de Cushamen (Chubut) entre los paralelos 42° y 42° 30' y los meridianos 70° y 71°. Rev. Asoc. Geol. Argent. 19 (2), 85–107.
von Gosen, W., 2009. Stages of Late Palaeozoic deformation and intrusive activity in the western part of the North Patagonian Massif (southern Argentina) and their geotectonic implications. Geological Magazine 146, 48–71. https://doi.org/10.1017/S0016756808005311.
White, R.W., Pomroy, N.E., Powell, R., 2005. An in situ metatexite-diatexite transition in upper amphibolite facies rocks from Broken Hill, Australia. Journal of Metamorphic Petrology 23, 579–602.
Winter, J., 2014. Principles of Igneous and Metamorphic Petrology, Second Edition. Pearson New International Edition. Pearson Education Limited, Edinburgh Gate, Harlow, UK.